Design of Low Reynolds Number Airfoils: Part I

W. Pfenninger* and C. S. Vemuru†
Analytical Services & Materials, Inc., Hampton, Virginia

The 9.5%-thick low Reynolds number (*Re*) airfoils ASM-LRN-003 and ASM-LRN-007 were designed for high section lift-to-drag ratios (C_L/C_{D_∞}) at $2.5\times10^5 < Re_c < 5.0\times10^5$, assuming laminar separation and transition control for minimum C_{D_∞} with turbulators. At the upper low-drag C_L limit ($C_L \approx 1.3$ to 1.4), 67–69%-chord laminar flow with substantial concave pressure recovery is expected on the upper surface. At $C_{L_{design}}$ the lower surface is fully laminar. To maximize (C_L/C_{D_∞}), the rear lower surface is undercut and aft-loaded, inducing a relatively strong local flow deceleration at lower C_L and correspondingly higher flight dynamic pressures. The resulting higher airloads on the flexible rear wing structure (similar to soaring bird wings with their chordwise feathers and quills) deflect and decamber the airfoil, thereby decreasing the pressure rise and enabling all laminar flow at lower C_L on the lower surface. An undercut front lower surface with a correspondingly sharper leading edge raises $(C_L/C_{D_\infty})_{max}$ further, narrowing, though, the low-drag C_L range. With optimum transition control, $(C_L/C_{D_\infty})_{max} = 120$ at $Re_c = 2.5\times10^5$ ($C_L = 1.40$) and 166 at $Re_c = 5.0\times10^5$ ($C_L = 1.35$) result, using Drela's code for airfoil ASM-LRN-003. The low-drag C_L range increases substantially by deflecting a 16%-chord cruise flap.

Nomenclature

A	= boundary-layer disturbance amplitude
A_0	= initial disturbance amplitude
b	= wingspan
C_{D_∞}	= profile drag coefficient
C_L	= lift coefficient
$C_{m_{c/4}}$	= airfoil pitching coefficient based on quarterchord
C_p	= surface static pressure coefficient, $=2p/\rho U_\infty^2$
c	= airfoil chord
D_i	= induced drag
L	= lift
M_∞	= freestream Mach number
n_{TS}	= logarithmic growth factor of amplified Tollmien-Schlicting-type boundary-layer disturbances, $=\ln(A/A_0)$
Re	= Reynolds number
Re_c	= Reynolds number based on chord
(t/c)	= airfoil thickness ratio
x	= chordwise distance
y	= vertical coordinate
α	= angle of attack
$\beta_{0.16}$	= deflection of 0.16-chord trailing edge
δ^*	= boundary-layer displacement thickness
θ	= boundary-layer momentum thickness
ν	= kinematic viscosity
ρ	= density

Subscripts

tr	= transition
TS	= Tollmien-Schlichting

Introduction and Problem Formulation

ATTEMPTS have been made to understand better the wing design of large soaring birds such as the condor or albatross.[1] Their wing chord Reynolds number is of the order $2.5\text{–}3.0\times10^5$ during static and dynamic soaring for the condor and albatross, respectively. The corresponding C_L seems to be close to the value for $(C_L/C_{D_\infty})_{max}$, taking the variation of C_{D_∞} with flight speed and Re_c into account ($Re_c \sim C_L^{-0.5}$). The variation of (C_L/C_{D_∞}) with C_L shows a wide optimum for well-designed low Reynolds number airfoils (Fig. 1). The bird wing may then be designed for other than pure aerodynamic performance considerations alone, such as takeoff, landing, or soaring in very tight thermals for the condor. Dynamic soaring requires a wide speed and C_L range with low C_{D_∞} for the albatross.

The question arises as to how the bird wings optimize (C_L/C_{D_∞}) at low Re_c; specifically, how they avoid excessive laminar separation bubble-induced pressure drag on the upper surface of their wings and especially how they minimize the chordwise extent of these bubbles to reduce the resulting wing pressure drag. A further question arises as to how the flexible chordwise structure of the bird wing may improve its low-drag C_L range at the low C_L limit.

Besides better understanding the wing design of large soaring birds, the development of low *Re* airfoils with high section lift-to-drag ratios becomes important for long-range and long-endurance high-altitude airplanes and remotely piloted vehi-

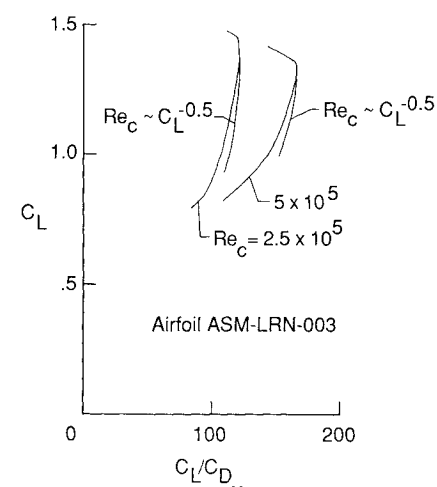

Fig. 1 Variation of C_L with $(C_L/C_{D\infty})$ for the ASM-LRN-003 airfoil.

Presented as Paper 88-0275 at the AIAA 6th Applied Aerodynamic Testing Conference, Williamsburg, VA, June 6–8, 1988; received June 25, 1988; revision received May 10, 1989.

*Senior Research Scientist. Fellow AIAA.
†Research Scientist. Member AIAA.

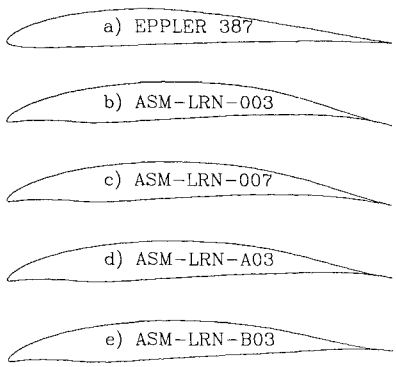

Fig. 2 Airfoil contours.

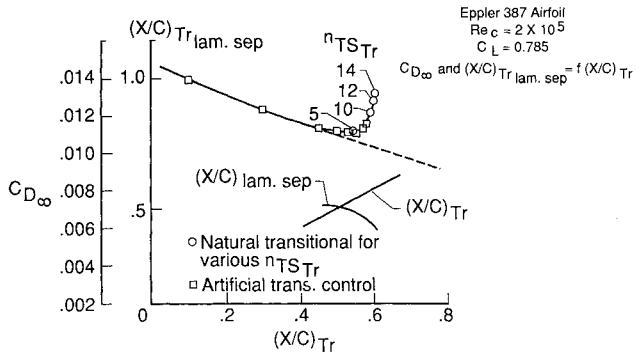

Fig. 3 Variation of C_{D_∞} with transition and laminar separation locations for E387 airfoil.

cles, man-powered airplanes (e.g., Daedalus), solar-powered high-altitude airplanes of low wing loading, model airplanes, etc. Equally important is the development of compressor and turbine bladings with high blade section lift-to-drag ratios and optimum control of laminar separation and transition in their low-pressure stages, where the blade chord Reynolds numbers may be uncomfortably low at high temperature of the laminar flow control (LFC) suction air at the suction compressor inlet of LFC airplanes. The Re_c of the suction compressor blades may be particularly low for supersonic LFC airplanes cruising at high altitudes. Artificial laminar separation and transition control on the suction compressor blading is then desirable.

Laminar Separation and Transition Control

Shallow laminar separation bubbles on the upper surface of low *Re* airfoils minimize laminar separation-induced pressure drag.[2,3] This is possible by avoiding an excessively convex upper surface in the transition zone, leading generally to a more rounded inviscid pressure distribution without a pronounced kink in the transition region and an excessively steep rear pressure rise.[3,4] Of course, thinner airfoils and lower C_L decrease the upper surface curvature and, thereby, thin the laminar separation bubble to reduce the bubble-induced pressure drag accordingly.

The Eppler E387 airfoil (Fig. 2a) is an example of this conservative approach.[5] Figure 3 shows C_{D_∞} and the start of laminar separation vs $(x/c)_{tr}$ both for the smooth airfoil at different $n_{TS_{tr}}$ values as well as for the case of forced transition at various (x/c) for $Re_c = 2.0 \times 10^5$ and $C_L \approx 0.78$ using Drela's code.[6] The experimental C_{D_∞} value of 0.0133, as measured by McGhee[7] in the low turbulence pressure tunnel (LTPT), agrees closely with the theoretical value of 0.0131, as obtained from the Drela analysis for the smooth airfoil with $n_{TS_{tr}} = 14$. (This drag was measued in a plane away from the location of the static pressure orifices to avoid orifice-induced disturbances). This high $n_{TS_{tr}}$ value is probably explained by the fact that n_{TS} grows at a particularly rapid rate toward the termination of the laminar separation bubble, as compared with the more gradual rise of n_{TS} on Viken's natural laminar flow airfoil[8] with $n_{TS_{tr}} \approx 11$ in the LTPT tunnel at higher Re_c. The experimentally observed location for the start of transition at $(x \times c)_{tr} = 0.62$ in the area away from the location of the static pressure orifices agrees closely with the theoretical value $[(x/c)_{tr} = 0.603$ for $n_{TS_{tr}} = 14]$.

The corresponding laminar separation bubble of the smooth airfoil extends (with $n_{TS_{tr}} = 14$) from $x/c = 0.40$ to 0.603. The agreement between the theoretical and experimental C_p distributions for the smooth airfoil E387 at $Re_c = 2.0 \times 10^5$ and $C_L = 0.785$ is excellent for $n_{TS_{tr}} = 10$ (Fig. 4). The agreement is somewhat less satisfactory for $n_{TS_{tr}} = 14$ (Fig. 5). Evidently, the disturbances introduced by the static pressure orifices must have caused a stronger local growth of TS disturbances to precipitate transition in this area at a lower maximum TS growth

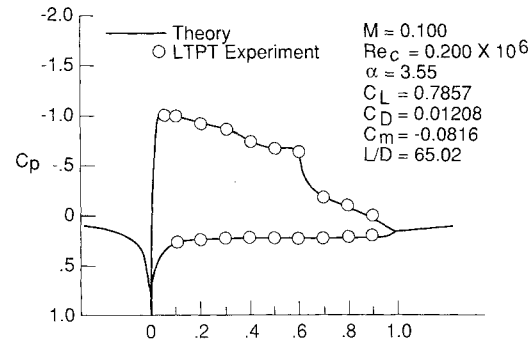

Fig. 4 Comparison of LTPT tunnel data and theoretical pressure distribution with $n_{TS_{tr}} = 10$ for E387 airfoil.

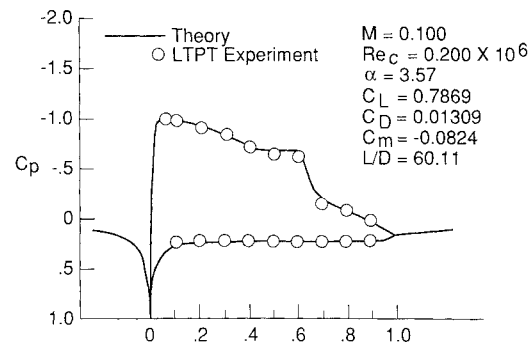

Fig. 5 Comparison of LTPT tunnel data and theoretical pressure distribution with $n_{TS_{tr}} = 14$ for E387 airfoil.

rate $n_{TS_{tr}} = 10$, as compared to 14 in the undisturbed portion of the wing. As a result, the laminar separation bubble in the zone of the static pressure orifices is shorter to reduce accordingly the local laminar separation-induced airfoil pressure and profile drag, as verified experimentally.[7] The Drela code thus gives an excellent correlation between theory and experiment for at least E387-type low Reynolds number airfoils.

The experimental profile drag polar of E387 in the LTPT tunnel at $Re_c = 2.0 \times 10^5$ shows some indentation at moderately high C_L,[7] indicating a noticeable laminar separation-induced pressure drag contribution even for this conservative low *Re* airfoil. Shifting transition further upstream to $(x/c)_{tr} \approx 0.55$ and thereby shortening the laminar separation bubble from $x/c = 0.48$ to 0.55 (accomplished either by means of suitable turbulators or raising the external disturbances such that $n_{TS_{tr}} = 5$) decreases C_{D_∞} at $Re_c = 2.0 \times 10^5$ and $C_L = 0.78$ from $C_{D_\infty} = 0.0131$ to 0.0111 (Drela analysis). Thus, laminar separation and transition control for laminar

separation-induced pressure drag minimization is desirable even for this conservatively designed E387 low *Re* airfoil at $Re_c = 2.0 \times 10^5$.

Enforcing transition further upstream at $(x/c)_{tr} = 0.50$ at the start of laminar separation does not decrease C_{D_∞} any further; the airfoil pressure drag resulting from the shallow laminar separation bubble with $(x/c)_{tr} = 0.55$ compensates for the additional turbulent skin friction between $x/c = 0.50$ and 0.55 with $(x/c)_{tr} = 0.50$.

Thus, one might reason that transition with a very weak and shallow laminar separation bubble would give the lowest profile drag.[2,3] This conclusion is correct for more conservatively designed laminar flow airfoils. It should, though, not be generalized: In principle, it is always possible to design natural laminar flow low *Re* airfoils with a sufficiently small adverse pressure gradient in the area shortly upstream of transition, such that the sum of airfoil pressure and friction drag contribution in the boundary-layer momentum equation in this area is minimized. The corresponding profile drag for $(x/c)_{tr} \geq 0.5$ would then be lower (dashed curve in Fig. 3) than airfoil E387 would indicate for the same transition location. Transition would then be enforced at the laminar separation point and the laminar separation bubble formation suppressed using suitable turbulators. If such laminar separation and transition control should prove feasible, the airfoil upper surface pressure distribution might be laid out from the start with a steeper rear pressure rise and correspondingly more extensive laminar flow and lower C_{D_∞} (dashed curve in Fig. 3). Admittedly, the profile drag is then more sensitive to the transition location, as compared with airfoil E387, requiring a correspondingly tighter transition control. Modern sailplane wings successfully use artificial laminar separation and transition control at $Re_c \approx 10^6$ to 2.0×10^6. For low *Re* airfoils with their particularly extensive laminar separation bubbles, such laminar separation and transition control should be even more beneficial and should, therefore, be considered from the start in their design. Such control is possible by using spanwise rows of three-dimensional surface or aerodynamic roughness elements (Noppenband[9]), bleed holes,[4,10] closely spaced suction holes,[11] etc. In contrast to bleed holes or three-dimensional surface roughness elements, the device drag of spanwise rows of suction holes is zero or negative.

Alternately, the upper surface boundary layer of low *Re* airfoils may be destabilized by generating dynamically highly unstable inflexional laminar boundary layers in instability zones or ramps with decelerated flow[5,12] or downstream of one or several two-dimensional backward-facing surface steps[4] or tape strips,[13,14] such that $n_{TS_{tr}}$ is reached around the start of laminar separation. Zig-zag tapes[15-17] are especially effective in this respect, since they distort TS disturbance vortices three-dimensionally to induce a particularly rapid TS disturbance vortex growth to transition within two to three TS wavelengths.[18] They can be considerably thinner for transition control[15-17] than two-dimensional tape strips to reduce their device drag accordingly.

Two-dimensional surface waves, as investigated by Pfenninger[4] on propeller blade airfoil 11 in Zurich (1942), can be used to prevent laminar separation bubble formation and excessive airfoil pressure drag at low Re_c. Sinusoidal surface waves of 25-mm wavelength and 0.4-mm amplitude were installed on both airfoil surfaces along the entire chord of 250 mm. They suppressed laminar separation and, thus, reduced C_{D_∞} substantially at $Re_c < 2.5 \times 10^5$, as compared with the smooth airfoil, which showed an extensive laminar separation bubble with a high pressure and profile drag at low Re_c. At high Re_c, though, the wavy airfoil experienced premature transition and a correspondingly increased drag.

Instead of using a wavy surface to destabilize the upper surface boundary layer and thereby shorten the laminar separation bubble, the upper surface in the region upstream of transition may be approximated by a series of straight lines with convex corners.

The question arises as to how to control transition within a given C_L and Re_c range. Pneumatic turbulators can be adjusted more easily to the particular external flow condition than mechanical ones and, therefore, appear preferable in this respect. Three-dimensional turbulators, causing transition directly, appear advantageous in view of the relatively short distance, l, between the turbulator and transition with $(Ul/\nu)_{tr} = 12{,}000$, as compared with 40,000 for two-dimensional turbulators. The resulting drag penalty with a fixed turbulator location is accordingly smaller than with two-dimensional turbulators for $Re_c > Re_{c_{design}}$. Especially attractive in this respect is boundary-layer suction through one or several rows of particularly closely spaced suction holes, resulting in a highly uniform transition front without a device drag.

The question arises as to how the wings of soaring birds cope with the laminar separation bubble problem on the upper wing surface. The bird wing seems to be laid out with excessive convex surface curvature in the likely transition region of the upper surface; the inviscid C_p distribution in this area is probably well rounded, thereby maintaining a relatively shallow laminar separation bubble and reducing laminar separation-induced pressure drag losses accordingly. In addition, the bird wing probably uses several methods to destabilize the upper surface boundary layer: the feathers overlap in the chordwise direction with a series of shallow backward-facing steps, which destabilize the boundary layer further downstream. Since the feather ends are rounded, the resulting surface steps are three-dimensional in the spanwise direction and, thus, distort accordingly TS disturbance vortices three-dimensionally, leading to a correspondingly more rapid TS disturbance vortex growth. It is not certain as to how far the bird feathers are porous to allow weak area blowing from the lower to the upper surface to destabilize the boundary layer of the upper surface. Aerodynamically, the surface of a bird wing is not really that smooth, being advantageous in introducing further disturbances into the boundary layer to precipitate transition and shorten the extent of laminar separation bubbles.

Similar design approaches, as for the ASM-LRN-010 of Ref. 19, were used to design the low *Re* airfoils ASM-LRN-003 and ASM-LRN-007. To simulate the conditions on large bird wings, ASM-LRN-003 was designed purposely with a relatively heavily aft-loaded undercut rear lower surface, leading to a correspondingly thin and flexible wing in the rear part of the airfoil.

Design Examples of Low *Re* Airfoils

As in the design of many high *Re* airfoils with extensive natural laminar flow, the upper and lower surfaces of low *Re* airfoils usually should be designed for the upper and lower low-drag C_L limits, respectively, possibly considering cruise flaps[4] or other types of variable camber to increase the low-drag bucket. The upper surface C_p distribution at the upper low-drag C_L limit should, therefore, be chosen such that the limiting TS disturbance growth at transition is reached at as high a C_L as possible, especially when $C_{L_{design}}$ closely approaches the upper low-drag C_L limit, and vice versa for the lower surface at a particularly low C_L. The question thus arises as to how best to stabilize the laminar boundary layer of the upper and lower surfaces with strongly decelerated flow at low Re_c. Reed[20] and Reed and Nayfeh[21] have shown that a laminar boundary layer is stabilized most effectively against amplified TS disturbances around their lower branch. Applying this principle to a natural laminar flow airfoil at $Re_c \approx 10^7$, Viken and Pfenninger were able to decrease n_{TS} by reducing the flow acceleration in the the front part of the airfoil, where TS disturbances are damped anyhow, and increasing instead the flow acceleration further downstream in the area where TS disturbances start growing, as compared with a continuous-flow acceleration.[8] The same principle may be applied to low *Re* airfoils, except that surprisingly strong laminar flow decelerations with sharp pressure minima are possible

at low Re_c at the endpoints of the low-drag bucket, before reaching limiting TS disturbance growth rates.

Airfoil ASM-LRN-003 ($t/c = 0.095$, Fig. 2b)

A particularly far aft rear pressure rise and transition with low C_{D_∞} is possible with optimum transition control for minimum C_{D_∞} by means of turbulators with negligible device drag. The rear lower surface is undercut and particularly heavily loaded (Fig. 6), compatible with full-chord laminar flow at higher C_L and lower Re_c. To add additional positive lift on the front lower surface and reduce slightly the peak velocities on the front upper surface at high C_L and decrease at the same time wing pitching moments, the front lower surface is undercut (apparently similar to eagle wings). The leading-edge thickness is thereby reduced, at the cost of a narrower low-drag bucket (as compared with airfoils without such an undercut front lower surface, see airfoil ASM-LRN-010 of Ref. 19).

Figure 6 shows C_p distributions for airfoil ASM-LRN-003 in inviscid as well as viscous flow at $Re_c = 2.5$ and 5.0×10^5 for various α and C_L with the corresponding values for C_{D_∞}, C_L, $C_{m_{c/4}}$, and (C_L/C_{D_∞}) within the low-drag $C_L$range, using Drela's analysis code with optimum transition control for minimum C_{D_∞}. Extensive laminar flow up to $x/c = 0.67$ thus appears feasible on the upper surface at $Re_c = 2.5$ and 5.0×10^5 at $\alpha = 5$ and 6 deg close to the upper low-drag C_L limit. The corresponding upper surface C_p distribution in this area shows a surprisingly strong "concave"-type flow deceleration downstream of a sharp pressure minimum located close to the leading edge. As a result of the far upstream location of this pressure minimum and the correspondingly thin local boundary layer, combined with the strongly "concave" pressure recovery further downstream and $U' = \partial U/\partial s$ decreasing about inversely proportional to the surface distance downstream of the pressure minimum, the corresponding local Pohlhausen parameters $\lambda_{\text{Pohlh}} = \delta^2 U/\nu$ are not excessively negative and the boundary-layer shape parameters $H = \delta^*/\theta$ are not appreciably larger than the Blasius flat-plate value of 2.59. Therefore, the laminar boundary layer in the front part of the upper surface is not as unstable at low Re_c as one might first expect, thereby enabling extensive laminar flow on the upper surface at low Re_c for $\alpha = 5$ and 6 deg. The growth of amplified TS disturbances for airfoil ASM-LRN-003 at $\alpha = 5$ deg and $Re_c = 5.0 \times 10^5$, using the SALLY code and Drela analysis, is discussed in the Appendix.

For a similar case, boundary-layer development calculations, solving the boundary-layer differential equations (Kaups-Cebeci code), gave δ^*/θ values that were about 0.01–0.03 higher than the Drela code values. With the concave laminar pressure rise on the upper surface at $\alpha = 5$ and 6 deg, the corresponding chordwise variation of δ^*/θ is surprisingly small; i.e., Drela's integral method with Falkner-Skan-type profiles should be reasonably accurate in predicting the laminar boundary-layer development for these cases.

Figure 7 shows the corresponding values of C_{D_∞} and (C_L/C_{D_∞}) as well as the transition location $(x/c)_T$ vs C_L for $Re_c = 2.5$ and 5.0×10^5, with $(C_L/C_{D_\infty})_{\max} = 120$ at $Re_c = 2.5 \times 10^5$ ($C_L = 1.4$) and 166 at $Re_c = 5.0 \times 10^5$ ($C_L = 1.35$). During flight at constant altitude $Re_c \sim C_L^{-0.5}$, leading to a flat optimum of (C_L/C_{D_∞}) vs C_L (Fig. 1). Figure 8 presents C_L vs α_∞in inviscid as well as viscous flow for $Re_c = 2.5$ and 5.0×10^5.

Minimum C_{D_∞} is obtained with transition on the upper surface around $0.68c$ to $0.70c$. The lower surface remains fully laminar at higher C_L. The increasingly strong flow deceleration on the lower surface at lower C_L, though, eventually moves transition upstream of the trailing edge and increases accordingly C_{D_∞} (at $C_L \leq 0.84$ for $Re_c = 2.5 \times 10^5$ and $C_L \leq 0.95$ for $Re_c = 5.0 \times 10^5$) (Figs. 6 and 7). As a result of the aft-loaded undercut rear lower surface, the rear part of airfoil ASM-LRN-003 is rather thin and flexible similar to the rather flimsy and flexible structure of the chordwise wing feathers of soaring birds. (Such thin trailing edges reduce the trailing-edge static pressure to alleviate the rear pressure recovery on the upper surface and, thereby, enable correspondingly higher C_L at design.) The local airloads in the rearmost part of the bird wing are carried by a single layer of feathers

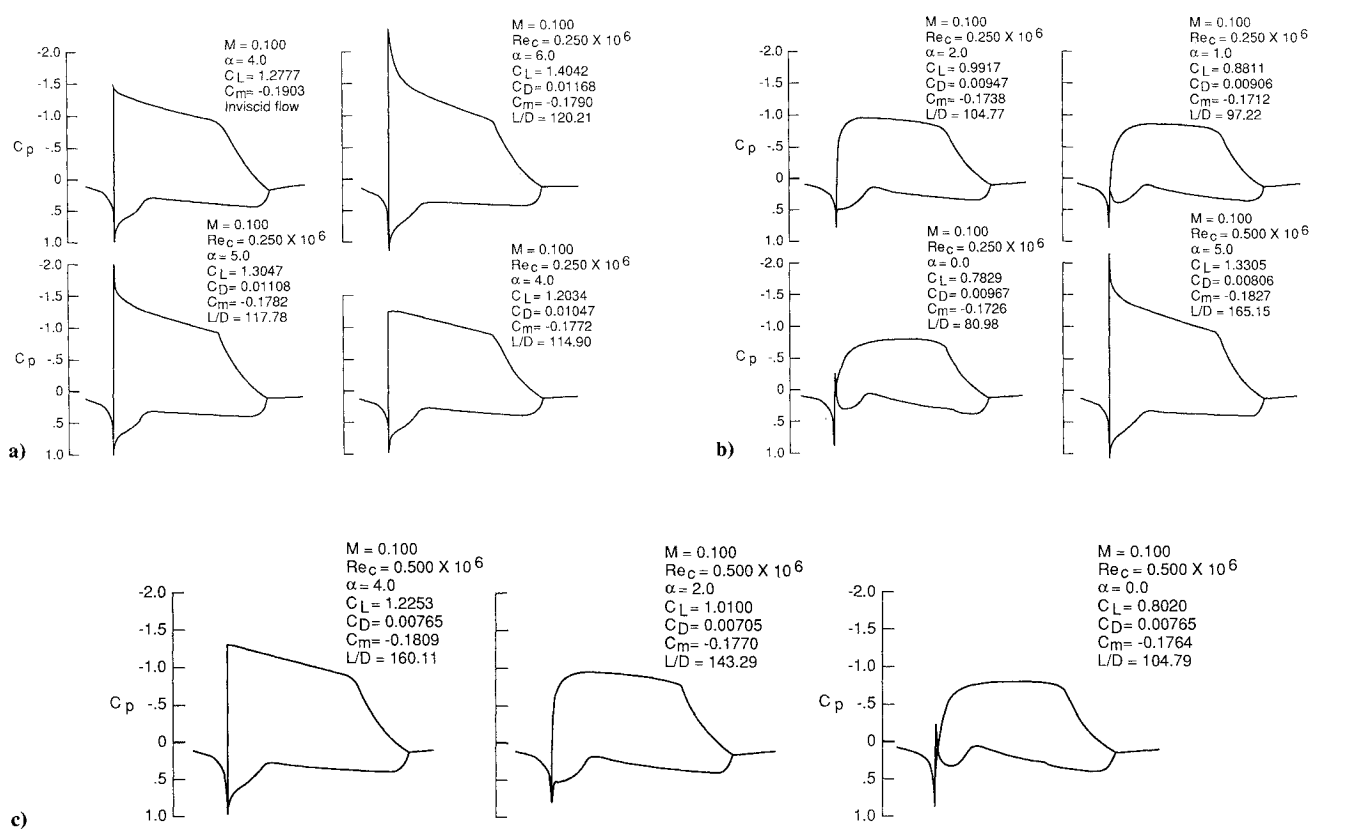

Fig. 6 Pressure distributions on ASM-LRN-003 airfoil at $Re_c = 2.5$ and 5.0×10^5, and different α.

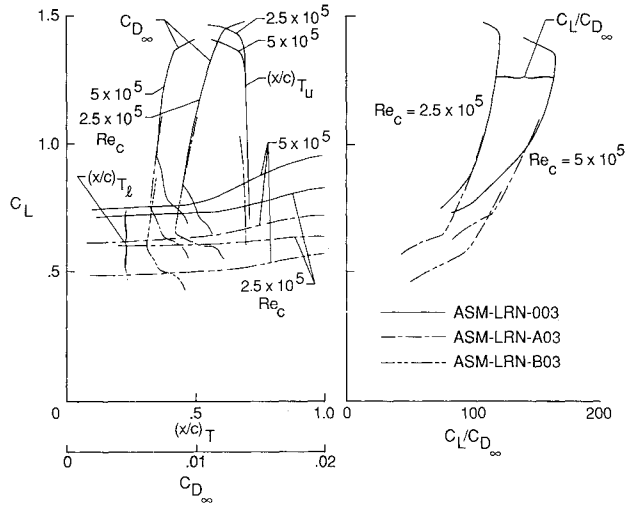

Fig. 7 Variation of C_L with C_{D_∞}, transition location, and (C_L/C_{D_∞}) for ASM-LRN-003, ASM-LRN-A03, and ASM-LRN-B03 airfoils.

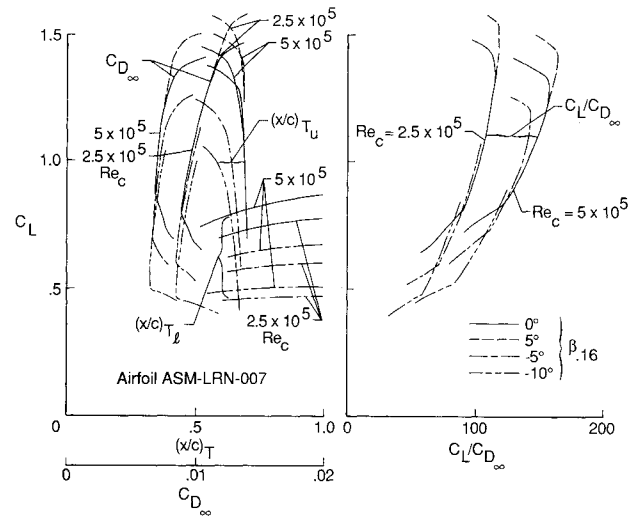

Fig. 9 Variation of C_L with C_{D_∞}, transition location, and (C_L/C_{D_∞}) for ASM-LRN-007 airfoil.

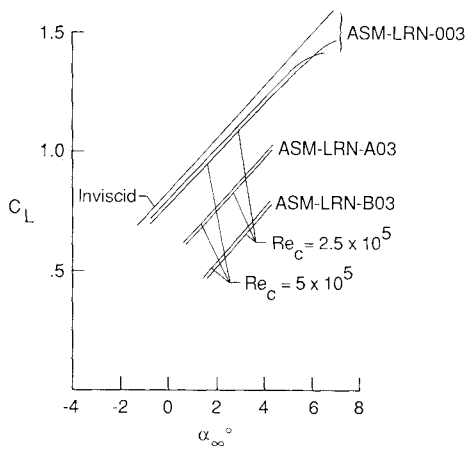

Fig. 8 Variation of C_L with α for ASM-LRN-003, ASM-LRN-A03, and ASM-LRN-B03 airfoils.

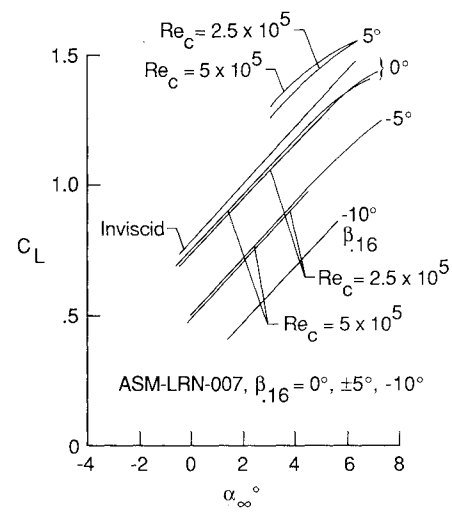

Fig. 10 Variation of C_L with α for ASM-LRN-007 airfoil.

and by two or more layers further upstream, while its quills transmit the airloads upstream to the main bird wing structure. Sufficient frictional damping among the different feather layers possibly delays wing flutter with the chordwise wing bending mode in combination with the spanwise wing bending and torsional modes.

The increased airloads in the rear part of the bird wing at lower C_L and correspondingly higher flight dynamic pressures decamber such a flexible bird wing at lower C_L. As a result, the flow deceleration on the lower surface decreases at lower C_L to enable an all-laminar lower surface. Thus, the bird wing with its flexible chordwise structure may have a built-in camber control at different C_L to increase its low-drag C_L range automatically. In a similar manner, one may use a thin, single sheet to carry the airloads of man-made machines in the rearmost part of airfoil ASM-LRN-003. Aerodynamically faired chordwise external stiffeners on the lower surface, equivalent to the quills of the chordwise bird feathers, may then transmit the airloads upstream to the main wing structure. The airfoil camber may thus decrease at the higher flight dynamic pressures associated with lower C_L. As a result, the flow deceleration on the rear lower surface decreases at lower C_L to shift transition back to the trailing edge and reduce C_{D_∞}, thereby improving the low-drag C_L range at its lower limit. As an example, airfoil ASM-LRN-003 was thus modified by deflecting the rear part of the airfoil between 0.60c and 1.0c upwards by $\Delta y/c = 0.1(x/c - 0.6)^2$ and $0.2(x/c - 0.6)^2$ (airfoils ASM-LRN-A03 and ASM-LRN-B03, Figs. 2d and 2e). Figures 7 and 8 show the corresponding $C_L(\alpha)$, as well as C_{D_∞}, (C_L/C_{D_∞}) and the transition location vs C_L of these modified airfoils with their reduced aft camber at $Re_c = 2.5$ and 5.0×10^5 for optimum transition control. Decambering, indeed, shifts the lower low-drag C_L limit to substantially lower C_L.

Airfoil ASM-LRN-007 ($t/c = 0.095$, Fig. 2c)

Variable trailing-edge camber, approached by deflecting a 16% trailing-edge cruise flap, improves the low-drag C_L range substantially. The profile drag polars, (C_L/C_{D_∞}) ratios, and transition locations vs C_L as well as C_L vs α_∞ are presented in Figs. 9 and 10 for optimum transition control at $Re_c = 2.5$ and 5.0×10^5 with cruise flap deflections $\beta_{0.16} = 0, -5, -10$, and 5 deg. As compared with airfoil ASM-LRN-003, the aft loading on the rear lower surface is reduced somewhat to thicken the rear part of the airfoil for flap installation; furthermore, to alleviate the laminar separation problem on the upper surface, its C_p distribution in the transition region is slightly more rounded. Combined with the reduced aft loading in the rearmost part of the lower surface, $(C_L/C_{D_\infty})_{max}$ decreases slightly for the unflapped airfoil ASM-LRN-007 to 117 at $Re_c = 2.5 \times 10^5$ (at $C_L = 1.37$) and 160 at $Re_c = 5.0 \times 10^5$ (at $C_L = 1.30$) (Fig. 9).

With increasing negative flap deflection ($\beta_{0.16} = -5$ deg and especially -10 deg), the flow deceleration on the lower surface decreases progressively to enable full-chord laminar flow on the lower surface down to $C_L \approx 0.5$ for $\beta_{0.16} = -10$ deg with correspondingly improved (C_L/C_{D_∞}) ratios at lower C_L, as compared with the unflapped airfoil (Fig. 9). Lowering the flap by 5 deg raises the upper low-drag C_L limit and $(C_L/C_{D_\infty})_{max}$ to 120 at $Re_c = 2.5 \times 10^5$ (at $C_L = 1.50$) and 166 at $Re_c = 5.0 \times 10^5$ (at $C_L = 1.42$) (Fig. 9).

Conclusions

Low Reynolds number airfoils ASM-LRN-003 and ASM-LRN-007 were designed for high section lift-to-drag ratios using Drela's design and analysis code. This was accomplished by maintaining close to 70% laminar flow on the upper and all-laminar flow on the lower surface at $C_L \approx 1.0$–1.3, assuming optimum laminar separation and transition control on the upper surface by suitable turbulators. Excellent agreement between the LTPT tunnel data on the E387 airfoil and the Drela code provides confidence in the performance of these airfoils with optimum transition control.

The airfoils ASM-LRN-007 and ASM-LRN-003 were designed optimally for high (C_L/C_{D_∞}) values at low Re_c, sacrificing a low-drag C_L range as a result of the aft-loaded lower surface and the relatively sharp leading edge with the concave front lower surface. The low-drag C_L range, of course, increases by avoiding an undercut front lower surface, using instead a more conventional front lower surface at some loss in $(C_L/C_{D_\infty})_{max}$.

If peak performance is particularly important, low Re airfoils with an undercut front lower surface and a correspondingly sharper leading edge, combined possibly with a more heavily loaded rear lower surface (using a thinner and more flexible rear airfoil), appear advantageous. Increased emphasis, though, must be given then to increase the low-drag C_L range by flap deflection or other types of variable trailing-edge geometry, combined possibly with low-drag suction on the lower surface.[19]

Appendix

The Drela analysis[6] takes the interaction of the boundary layer with the external flow into account in analyzing the C_p distribution, applying an integral method with "similar" Falkner-Skan-type solutions for the laminar boundary-layer development and using Tollmien-Schlichting stability results for the equivalent Falkner-Skan boundary-layer profiles to calculate the TS disturbance growth, assuming various n_{TS} values (typically 9) at transition. A Kaups-Cebeci[22] and SALLY analysis[22,23] for the upper surface C_p distribution of the low Re airfoil ASM-LRN-003 at $\alpha = 5$ deg and $Re_c = 5.0 \times 10^5$ with transition at $0.65c$ gave $n_{TS} \approx 11.5$ (Fig. A1), as compared with $n_{TS} = 9$ used in the Drela code. Despite the severe local flow deceleration on the front upper surface, the most strongly amplified TS disturbances are damped within the first 10% of the chord (Fig. 10). For the solution of the turbulent boundary-layer development, Drela uses eddy-viscosity concepts and integral methods.

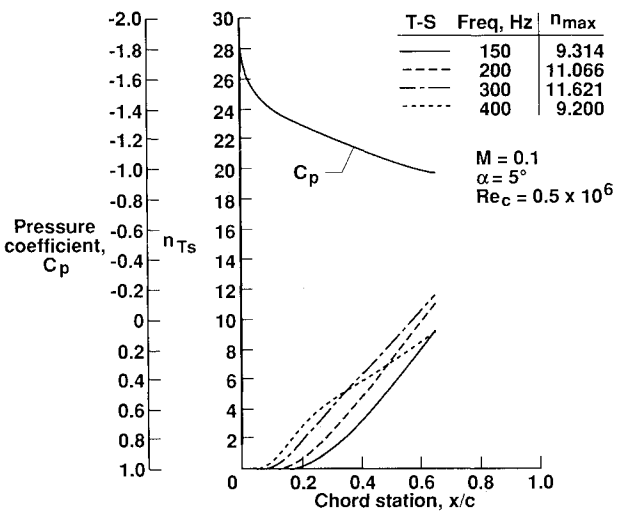

Fig. A1 Tollmien-Schlichting boundary-layer disturbance growth factors on the upper surface of the ASM-LRN-003 airfoil at $Re_c = 0.5 \times 10^6$ and $\alpha = 5$ deg.

Acknowledgments

The authors wish to express their sincere appreciation to Dr. Mark Drela of the Massachusetts Institute of Technology for his design and analysis code, which gives good accuracy at surprisingly modest efforts. The authors would also like to thank Jerry Hefner, Assistant Division Chief of Fluid Mechanics Division, and Richard Wagner and Dal Maddalon of the Laminar Flow Control Project Office for their support. This work was sponsored by the NASA Langley Research Center under Contract NAS1-18235.

References

[1]McMasters, J. H., "Reflections of a Paleo-Aerodynamicist," AIAA Paper 84-2167, Aug. 1984.

[2]Wortmann, F. X., "A Contribution to the Design of Laminar Profiles for Gliders and Helicopters," *Zeitschrift Flugwissenschaften,* Vol. 3, No. 10, 1955.

[3]Drela, M., "Low Reynolds Number Airfoil Design for the M.I.T. Daedalus Prototype: A Case Study," *Journal of Aircraft,* Vol. 25, Aug. 1988, pp. 724–732.

[4]Pfenninger, W., "Untersuchungen uber Reibungs-verminderungen an Tragflugeln, insbesondere mit Hilfe von Grenzschichtabsaugung," Institute for Aerodynamics, ETH, Zurich, Mitteilung 13, 1946.

[5]Eppler, R. and Somers, D., "Airfoil Design for Reynolds Numbers between 50,000 and 500,000," *Proceedings of the Conference on Low Reynolds Number Airfoils,* UNDAS-CP-77B123, June 1985.

[6]Drela, M., "Two-Dimensional Transonic Aerodynamic Design and Analysis Using the Euler Equations," Ph.D. Thesis, Massachusetts Institute of Technology, Cambridge, MA, 1985.

[7]McGhee, R. J., Jones, G. S., and Jouty, R., "Performance Characteristics from Wind Tunnel Tests of a Low Reynolds Number Airfoil," AIAA Paper 88-0607, Jan. 1988.

[8]Viken, J. K., "Aerodynamic Design Considerations and Theoretical Results for a High Reynolds Number Natural Laminar Flow Airfoil," Master's Thesis, George Washington Univ., Washington, DC, Jan. 1983.

[9]Althaus, D., "Influencing Transition on Airfoils," 17th Ostiv Congress, Paderborn, 1981.

[10]Horstmann, K. H. and Quast, A., "Drag Reduction by Means of Pneumatic Turbulators," DFVLR-FB-81-33, Braunschweig, FRG 1982.

[11]Goldsmith, J., "Critical Laminar Suction Parameters for Suction into an Isolated Hole or a Single Row of Holes," Northrop Corp., Rept. BLC-95, NAI-57-529, Feb. 1957.

[12]Wortmann, F. X., "Experimental Investigations on New Laminar Profiles for Gliders and Helicopters," *Zeitschrift Flugwissenschaften,* Vol. 5, No. 8, 1957.

[13]Pfenninger, W., "Experimental Investigation of an Airfoil with High Lift to Drag Ratios at Low Reynolds Numbers," Northrop, BLC Rept. 84 Corp., NAI 560188, 1956.

[14]Mangalam, S. M., Bar-sever, A., Zaman, K. M., and Harvey, W. D., "Transition and Separation Control on a Low Reynolds Number Airfoil," Proceedings of the Royal Aeronautical Society, International Conference on Aerodynamics at Low Reynolds Numbers, Proceedings of the Royal Aeronautical Society, London, England, Oct. 1986.

[15]Hama, F. R., "An Efficient Tripping Device," *Journal of Aeronautical Sciences,* March 1957.

[16]Hegarty, J. C. and Hama, F. R., "Further Investigations of the Triangular-Patch Stimulator," TN BN-107, AFOSR TN-57-616, ASTIA AD-136-605, June 1957.

[17]Van Ingen, J. L. and Boermans, L. M. M., "Research on Laminar Separation Bubbles at Delft University of Technology in Relation

to Low Reynolds Number Airfoil Aerodynamics," *Proceedings of the Conference on Low Reynolds Number Airfoils,* UNDAS-CP-77B123, June 1985.

[18]Saric, W. S. and Reynolds, G. S., "Experiments on the Stability of Nonlinear Waves in a Boundary Layer," Laminar-Turbulent Transition; IUTAM Symposium on Transition, Stuttgart, FRG, Sept. 1979.

[19]Pfenninger, W., Vemuru, C S., Mangalam, S. M., and Evangelista, R., "Design of Low Reynolds Number Airfoils – II," AIAA Paper 88-3764, July 1988.

[20]Reed, H. L., "The Tollmien-Schlichting Instability of Laminar Viscous Flows," Ph.D. Thesis, Virginia Polytechnic Institute and State University, Blacksburg, VA, Dec. 1981.

[21]Reed, H. L. and Nayfeh, A. H., "Stability of Flow over Plates with Porous Suction Strips," AIAA Paper 81-1280, June 1981.

[22]Kaups, K. and Cebeci, T., "Compressible Laminar Boundary Layers with Suction on Swept and Tapered Wings," *Journal of Aircraft,* Vol. 14, July 1977.

[23]Srokowski, A. J. and Orszag, S. A., "Mass Flow Requirements for LFC Wing Design," AIAA Paper 77-1222, Aug. 1977.